The Astrophysical Journal, 693:839–846, 2009 March 1 doi:10.1088/0004-637X/693/1/839

EFFECT OF HELIUM SEDIMENTATION ON X-RAY MEASUREMENTS OF GALAXY CLUSTERS

Fang Peng[1] and Daisuke Nagai[1,2,3]
[1] Theoretical Astrophysics, California Institute of Technology, Mail Code 130-33, Pasadena, CA 91125, USA; fpeng@caltech.edu
[2] Department of Physics, Yale University, New Haven, CT 06520, USA
[3] Yale Center for Astronomy & Astrophysics, Yale University, New Haven, CT 06520, USA; daisuke.nagai@yale.edu
Received 2008 August 27; accepted 2008 November 13; published 2009 March 3

ABSTRACT

The uniformity of the helium-to-hydrogen (He-to-H) abundance ratio in the X-ray emitting intracluster medium (ICM) is one of the commonly adopted assumptions in X-ray analyses of galaxy clusters and cosmological constraints derived from these measurements. In this paper, we investigate the effect of He sedimentation on X-ray measurements of galaxy clusters in order to assess this assumption and associated systematic uncertainties. By solving a set of flow equations for a H–He plasma, we show that the He-to-H mass ratio is significantly enhanced in the inner regions of clusters. The effect of He sedimentation, if not accounted for, introduces systematic biases in observable properties of clusters derived using X-ray observations. We show that these biases also introduce an apparent evolution in the observed gas mass fractions of X-ray luminous, dynamically relaxed clusters and hence biases in observational constraints on the dark energy equation of state parameter, w, derived from the cluster distance-redshift relation. The Hubble parameter derived from the combination of X-ray and Sunyaev–Zel'dovich effect measurements is affected by the He sedimentation process as well. Future measurements aiming to constrain w or H_0 to better than 10% may need to take into account the effect of He sedimentation. We propose that the evolution of gas mass fraction in the inner regions of clusters should provide unique observational diagnostics of the He sedimentation process.

Key words: cosmological parameters – diffusion – X-rays: galaxies: clusters

Online-only material: color figures

1. INTRODUCTION

Clusters of galaxies are powerful cosmological probes and have the potential to constrain properties of dark energy and dark matter. Recent developments in X-ray observations of galaxy clusters have produced a large statistical sample of clusters and have started delivering powerful cosmological constraints (Allen et al. 2004, 2008; Mantz et al. 2008; Vikhlinin et al. 2009) that are complimentary to and competitive with other techniques (e.g., supernova, baryon acoustic oscillation, and weak lensing). This has motivated construction of the next generation of X-ray satellite missions (e.g., *eROSITA*) to push the precision cosmological measurements based on large X-ray cluster surveys. However, in the era of precision cosmology, the use of clusters as sensitive cosmological probes requires solid understanding of cluster gas physics, testing of simplifying assumptions, and assessing associated systematic uncertainties.

One of the commonly adopted assumptions in X-ray cluster analyses include the uniformity of the helium-to-hydrogen (He-to-H) abundance ratio with nearly primordial composition in the X-ray emitting intracluster medium (ICM). At present, there is no observational test of this assumption, since both H and He in the ICM are fully ionized, which makes it difficult to measure their abundances using traditional spectroscopic techniques. Theoretically, on the other hand, it has long been suggested that heavier He nuclei slowly settle in the potential well of galaxy clusters and cause a concentration of He toward their center (Abramopoulos et al. 1981; Gilfanov & Syunyaev 1984; Qin & Wu 2000; Chuzhoy & Nusser 2003; Chuzhoy & Loeb 2004; Ettori & Fabian 2006). In the era of precision cosmology, this could be a source of significant systematic uncertainties in X-ray measurements of galaxy clusters and cosmological parameters derived from these measurements (Markevitch 2007).

Thus, the primary goal of the present work is to assess the validity of this assumption and the associated systematic uncertainties in X-ray measurements of key cluster properties as well as cosmological parameters derived from these observations. In this work, we investigate the effects of He sedimentation on X-ray measurements of galaxy clusters by solving a set of diffusion equations for a H–He plasma in the ICM. By taking into account observed temperature profiles obtained by recent X-ray observations (Vikhlinin et al. 2006; Pratt et al. 2007; Leccardi & Molendi 2008; George et al. 2009), we show that the observed temperature drop in the cluster outskirts leads to a significant suppression of He sedimentation, compared to the results based on the isothermal cluster model (Chuzhoy & Loeb 2004). Our analysis indicates that the He sedimentation has negligible effect on X-ray measurements in the outer regions of clusters (e.g., r_{500}), and it does not affect cluster mass measurements obtained at the sufficiently large cluster radius. The effect of He sedimentation, on the other hand, introduces increasingly larger biases in X-ray measurements in the inner regions and could affect cosmological constraints, including the dark energy equation of state parameter w derived from distance–redshift relation as well as H_0 derived from the combination of X-ray and Sunyaev–Zel'dovich effect (SZE).

The paper is organized as follows. In Section 2, we describe the dependence of X-ray clusters measurements on He abundance in the ICM. The physics of He sedimentation and cluster models are discussed in Section 3. In Section 4, we present results of our He sedimentation calculations and investigate their effects on cluster properties and cosmological constraints derived from X-ray cluster observations. The main conclusions are summarized in Section 6.

2. EFFECT OF He ABUNDANCE ON X-RAY MEASUREMENTS

The observed X-ray surface brightness of a cluster is primarily from bremsstrahlung continuum emission of electrons scattering off of protons and He nuclei, which is given by the integral of the emission along the line of sight,

$$S_X \propto \int dl\,(n_e n_{\rm p}\Lambda_{e{\rm p}} + n_e n_{\rm He}\Lambda_{e{\rm He}}) \tag{1}$$

$$\propto n_{\rm p}^2(1+2x)(1+4x)\Lambda_{e{\rm p}}, \tag{2}$$

where $x \equiv n_{\rm He}/n_{\rm p}$ is the He-to-H abundance ratio and Λ_{ei} is the band-limited cooling function resulting from free–free emission of electrons scattering off ion species i, which is proportional to Z_i^2. The derivation of the second expression takes into account the charge dependence of cooling function and the fact that the number density of electron is given by $n_e = n_{\rm p} + 2n_{\rm He} = n_{\rm p}(1+2x)$. Since S_X is observed and fixed, the proton number density $n_{\rm p}$ inferred from X-ray observations depends on x, as $n_{\rm p} \propto 1/\sqrt{(1+2x)(1+4x)}$. The derived gas mass density therefore depends on x as,

$$\rho_{\rm gas} \propto n_{\rm p} + 4n_{\rm He} \propto \left(\frac{1+4x}{1+2x}\right)^{1/2}. \tag{3}$$

The gas mass $M_{\rm gas}$ is the volume integral of Equation (3). The hydrostatic mass profile of a spherically symmetric cluster depends on the local value of He abundance through the mean molecular weight of particles μ,

$$M_{\rm tot}(<r) \propto \frac{rT_e}{\mu}\frac{d\log\rho_{\rm gas}}{d\log r} \propto \frac{1}{\mu} = \frac{2+3x}{1+4x}. \tag{4}$$

Note that the hydrostatic mass at a fixed mean overdensity, Δ, is given by $M_\Delta \propto (T_e/\mu)^{3/2}$. The gas mass fraction is then defined as $f_{\rm gas} \equiv M_{\rm gas}/M_{\rm tot}$.

For the primordial abundance ($X = 0.75$, $Y = 0.25$ by mass), the He-to-H abundance ratio is $x = 0.083$ and the mean molecular weight is $\mu = 0.59$. If, for example, the He-to-H abundance ratio is enhanced by a factor of 2 from the primordial value, the analysis based on the assumption of the primordial abundance causes an underestimate of $\rho_{\rm gas}$ by 5% and an overestimate of $M_{\rm tot}$ by 12%.

3. HELIUM SEDIMENTATION IN X-RAY CUSTERS

3.1. Diffusion Equations

Particle diffusion in clusters is characterized by the Burgers equations of a multicomponent fluid (Burgers 1969). Each species s obeys an equation of continuity and momentum conservation,

$$\frac{\partial n_s}{\partial t} + \frac{1}{r^2}\frac{\partial(r^2 n_s u_s)}{\partial r} = 0, \tag{5}$$

$$\frac{\partial P_s}{\partial r} + n_s A_s m_{\rm p} g - n_s Z_s e E = \sum_t K_{st}(w_t - w_s). \tag{6}$$

Here the species s has mass $A_s m_{\rm p}$, charge $Z_s e$, density n_s, partial pressure P_s, and velocity u_s, where $m_{\rm p}$ is the proton mass. The center of mass of a fluid element moves with a velocity $u = \sum_s n_s A_s u_s \big/ \sum_s n_s A_s$. The differential, or diffusion, velocity between species s and the fluid element is then $w_s = u_s - u$. These diffusion velocities satisfy mass and charge conservation,

$$\sum_s A_s n_s w_s = 0, \tag{7}$$

$$\sum_s Z_s n_s w_s = 0. \tag{8}$$

Note that the summations include both ions and electrons. To satisfy these conservation laws, for each sinking helium nuclei, there are roughly four protons and two electrons that float up.

Equation (6) describes forces acting on a species s, and it is the balance of these forces that ultimately determines the rate of sedimentation. For a sinking He nucleus, the gravitational force (g) is counteracted by three types of forces provided by the induced electric field (E), the pressure gradient (dP_s/dr) of the ICM, and the drag force due to collisions with surrounding particles. Note that we neglected small terms including the inertial term (du_s/dt) and the shear stresses (or viscosity) due to collisions among the same species. We also neglected terms related to the coupling of thermal and particle diffusions, which lead to an underestimate of the He-to-H mass ratio by $\lesssim 20\%$ in the radial range considered in this work (see Section 5).

Note that the sedimentation destroys hydrostatic equilibrium since redistribution of particles introduces a temporal change in the total gas pressure. However, hydrostatic equilibrium can be restored quickly. This equilibrium restoring acquires a net inflow with a mean velocity u,

$$\frac{du}{dt} = -\frac{1}{\rho_{\rm gas}}\frac{\partial P_{\rm gas}}{\partial r} - g, \tag{9}$$

where $P_{\rm gas} = \sum_s n_s k_{\rm B} T$ is the total gas pressure for ideal gas, and $\rho_{\rm gas} = \sum_s n_s A_s m_u$ is the gas density. Equations (5)–(9) describe the process of particle diffusion in the ICM.

3.2. Resistance Coefficient

When the plasma is sufficiently rarefied, which is the case for the ICM, particle pairs interact via a pure Coulomb potential. In the absence of magnetic field and turbulence, the resistance coefficient is given by Chapman & Cowling (1952) as

$$K_{st}^{B=0} \cong \frac{4\sqrt{2\pi}}{3}\frac{e^4 Z_s^2 Z_t^2 \mu_{st}^{1/2}}{(k_{\rm B}T)^{3/2}} n_s n_t \ln\Lambda_{st}, \tag{10}$$

where $\mu_{st} = A_s A_t m_{\rm p}/(A_s + A_t)$ is the reduced mass of species s and t, and a typical value of the Coulomb logarithm is $\ln\Lambda_{st} \simeq 40$ for the H–He plasma in the ICM. Resistance coefficient describes the momentum transfer rate of species s per unit volume due to collisions with species t (in units of $\mathrm{g\,cm^{-3}\,s^{-1}}$). The resistance coefficient, $K_{st} \propto T^{-3/2}$, is inversely proportional to the ICM temperature. Therefore, particle transport is more efficient in the ICM with higher temperature. Note that heat transport via the same particle collision physics gives that the thermal conductivity depends on T as $\kappa \propto T^{5/2}$.

However, magnetic field and turbulence, present in real clusters, can significantly modify the resistance coefficients. To date, theoretical work on this subject has predicted a wide range of the magnetic suppression factor, $f_B \equiv \kappa/\kappa_{\rm Sp} \sim 0.1 - 1$, where $\kappa_{\rm Sp}$ is the Spitzer thermal conductivity (Spitzer 1962), depending sensitively on the strength and the geometry of magnetic field as well as the nature of MHD turbulence. In the

case of a tangled magnetic field, the thermal conductivity may be moderately suppressed ($f_B \sim 0.1 - 0.2$) relative to the Spitzer value (Narayan & Medvedev 2001; Chandran & Maron 2004). Magnetothermal instability tends to drive magnetic field lines to a radial direction, which gives the suppression of $f_B \gtrsim 0.4$ (Parrish et al. 2008). It was also suggested that MHD turbulence may provide a magnetic suppression factor of order unity (Cho & Lazarian 2004; Lazarian 2007).

Observationally, one can use the strength of observed temperature gradients in the ICM to constrain the efficiency of thermal conductivity. Observed large-scale, negative ICM temperature gradients set the upper limit on the thermal conductivity, $f_B \lesssim 0.2$ for a $T_X = 10$ keV cluster with a typical age of 7 Gyr (Loeb 2002). Observations of A754 also yield a suppression factor $f_B < 0.1$ for the bulk of the ICM (Markevitch 2003). The width of cold fronts observed by recent X-ray observations suggests a considerably smaller suppression factor ($f_B \ll 0.1$) (see Markevitch & Vikhlinin 2007 for a review). This, however, is a local constraint that is not applicable to a cluster as a whole. One might also imagine that the abundance profile of heavy nuclei (e.g., Fe) with X-ray emission lines may provide further insights into the efficiency of particle diffusion. Though possible in principle, interpretation of the abundance profile is complicated by the fact that the ICM is enriched continuously by stripping of metal-enriched gas from cluster galaxies, and that the process of sedimentation is generally slower for heavier nuclei.

Given the current large uncertainties in diffusion coefficients due to the lack of knowledge on magnetic field and turbulence in the ICM, we parametrize the effective resistance coefficients as $K_{st} = f_B^{-1} K_{st}^{B=0}$, where we take f_B as a free parameter. In order to illustrate how our results depend on the suppression factor, we consider two cases with $f_B = 1$ (unmagnetized) and 0.2 (tangled magnetic field). The former should be taken as an extreme model, while the latter roughly corresponds to the current observational limit discussed above. Note, however, that all current observations are consistent with $f_B = 0$ (conduction fully suppressed). We therefore caution that f_B may be orders of magnitude below unity.

3.3. Sedimentation Velocity

To develop physical insights into the process of He sedimentation, it is useful to consider a drift velocity of a trace He particle in a background of hydrogen, i.e, $n_{\rm p} \gg n_{\rm He}$ and $w_{\rm p} = 0$. In this limiting case, Equations (6) for the two species are decoupled. The right-hand side of the equations for H vanishes, thereby fixing an electric field, $eE = 0.5\, m_{\rm p} g$. Substituting E into the equation of motion for He, we obtain the sedimentation velocity of He nuclei as $w_{\rm He} = 3\, m_{\rm p} g n_{\rm He} / K_{\rm pHe}$, which gives

$$w_{\rm He} \simeq 80\,{\rm km\,s^{-1}}\, f_B \times \left(\frac{T}{10\,{\rm keV}}\right)^{3/2} \left(\frac{g}{10^{-7.5}\,{\rm cm\,s^{-2}}}\right) \left(\frac{n_{\rm p}}{10^{-3}\,{\rm cm^{-3}}}\right)^{-1} \quad (11)$$

where the induced electric field counteracts gravity and suppresses the sedimentation speed by 25%. At a fixed density, the sedimentation velocity is generally larger for higher temperature (T) and gravity (g). Note that the pressure gradient (dP/dr) term in Equation (6) further suppresses the sedimentation process. Typical sedimentation timescale in clusters is generally longer than the Hubble time. The equilibrium distributions to the Burgers equation (Abramopoulos et al. 1981; Qin & Wu 2000; Chuzhoy & Nusser 2003) are therefore not applicable for clusters. Instead, a full time-dependent calculation is required for this analysis.

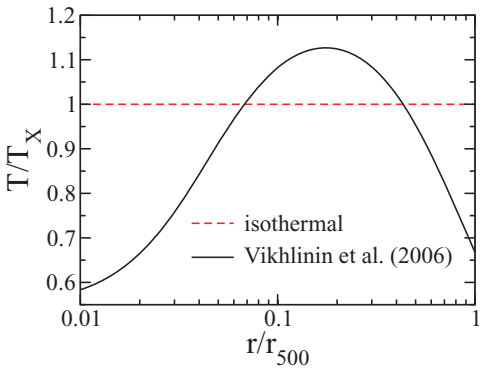

Figure 1. Temperature profiles of X-ray clusters used in our models: isothermal temperature profile (dashed line) and observed temperature profile obtained by Vikhlinin et al. (2006) (solid line).

(A color version of this figure is available in the online journal.)

3.4. Cluster Models and Initial Conditions

We set up cluster models and initial conditions as follows. Initially, we assume that the ICM consists of a primordial H and He plasma uniformly throughout clusters. We ignore the contribution of heavier elements of $Z > 2$.

For the total mass distribution, we adopt the Navarro–Frenk–White (NFW) density profile (Navarro et al. 1997)

$$\rho(r) = \frac{\rho_s}{x'(1+x')^2}, \quad (12)$$

where $x' \equiv r/r_s$, r_s is a scale radius, and ρ_s is a normalization constant. Mass enclosed within a radius r is then given by $M(x') = 4\pi\rho_s r_s^3[\ln(1+x') - x'/(1+x')]$. Throughout this work, we define the cluster mass to be $M_\Delta = (4\pi/3) r_\Delta^3 \Delta\, \rho_{\rm crit}$, where r_Δ is a radius of a spherical region within which the mean enclosed mass density is Δ times the critical density of the universe $\rho_{\rm crit}$. We adopt $\Delta = 500$ and the concentration $c_{500} \equiv r_{500}/r_s = 4$ (V06). We also consider $\Delta = 2500$, where some of the X-ray measurements are also made. In this cluster model, $r_{2500}/r_{500} = 0.46$.

We consider two ICM temperature models: (1) the isothermal temperature profile $T(r) = T_X$, and (2) the observed temperature profile obtained with deep *Chandra* observations of nearby relaxed clusters (V06) given by

$$\frac{T(r)}{T_X} = 1.216 \frac{(\tilde{x}/0.045)^{1.9} + 0.45}{(\tilde{x}/0.045)^{1.9} + 1} \frac{1}{[1 + (\tilde{x}/0.6)^2]^{0.45}}, \quad (13)$$

where $\tilde{x} = r/r_{500}$, and T_X is the X-ray spectral temperature, which is related to $M_{500} = M_5 (T_X/5\ {\rm keV})^\alpha$, where $M_5 = 2.89 \times 10^{14}\, h^{-1}\, M_\odot$ and $\alpha = 1.58$ (V06). For an illustration, we plot these ICM temperature profiles in Figure 1. The observed temperature peaks around $r/r_{500} \simeq 0.2$, and decreases at both inner and outer radii. For example, the temperature drops by nearly a factor of 2 from the peak value at $r/r_{500} = 0.01$ and 1.

We set up the initial gas distribution by assuming hydrostatic equilibrium of the ICM in the potential well of clusters dominated by dark matter,

$$\frac{k_{\rm B}}{\mu m_u} \frac{d(\rho_{\rm gas} T)}{dr} = -\rho_{\rm gas} g(r), \quad (14)$$

where the gravitational acceleration at a radius r is $g(r) \equiv GM(r)/r^2$. For each temperature profile $T(r)$, we derive the initial gas density profile as,

$$\rho_{\rm gas}(r) = \rho_{\rm gas,0}\left(\frac{T_0}{T(r)}\right)\exp\left(-\frac{\mu m_{\rm p}}{k_{\rm B}}\int_0^r \frac{g(r')}{T(r')}dr'\right), \quad (15)$$

where the central density $\rho_{\rm gas,0}$ is normalized by requiring $M_{\rm gas}/M(r_{500}) \equiv f_{\rm gas,500} = 0.15$ (V06), and T_0 is the central temperature for each ICM temperature model. For isothermal case, the density profile reproduces the analytical form given by $\rho_{\rm gas}(r) = \rho_{\rm gas,0}\exp(-\eta\mu)(1+x')^{\eta\mu/x'}$ with $\eta = 4\pi G m_{\rm p}\rho_s r_s^2/(k_{\rm B}T_X)$ (Makino et al. 1998).

Finally, we consider two types of mass accretion histories (MAHs) of clusters: (1) a static cluster with a fixed mass, (2) the MAHs of cluster-size halos calibrated with N-body simulations of cluster formation. For the latter, we adopt an analytical expression of averaged MAHs of halos given by van den Bosch (2002),

$$\log\left(\frac{M}{M_0}\right) = -0.301\left[\frac{\log(1+z)}{\log(1+z_f)}\right]^{\nu}, \quad (16)$$

where M_0 is the cluster mass at present time, z_f is the formation redshift defined as $M(z_f)/M_0 = 0.5$, and ν is a parameter that determines the shape of MAHs of dark matter halos, and it is strongly correlated with z_f. This functional form provides a reasonable description of the MAHs of simulated clusters for a typical value of ν in the range of 1.4–2.3 (Tasitsiomi et al. 2004) and an average formation redshift of $\langle z_f\rangle \simeq 0.6$ (Cohn & White 2005, see also Berrier et al. 2009).[4] The points that are particularly relevant for this work are that a typical present-day cluster grows by a factor of 2 in mass in the past ≈ 6 Gyr since $z \approx 0.6$, while an equal-mass cluster at higher redshift ($z = 1$) forms in a considerably shorter timescale ($\approx 1-2$ Gyr). This suggests that the high-z clusters are generally much less affected by the process of He sedimentation than their low-redshift counterparts. In Section 4.1–4.3, we use the simple static cluster model to investigate the dependence of the He sedimentation efficiency on some of the key cluster parameters, including the temperature, the age, and the magnetic suppression factor. In Section 4.4, we use the realistic MAHs to investigate evolution in X-ray observable properties with redshift. Throughout this work, we use cosmological parameters: $\Omega_{\rm M} = 0.3$, $\Omega_\Lambda = 0.7$, $\Omega_{\rm b} = 0.0462$, and $h = 0.7$ (Komatsu et al. 2009).

4. RESULTS

4.1. Spatial Distribution and Evolution of He Abundance

Starting from the initial cluster model described in Section 3.4, we follow the diffusion process in the H and He plasma by solving Equations (5)–(9) numerically. At each time step, Equations (6)–(8) are solved to obtain diffusion velocities (w_s) for H, He and electrons as well as electric field (E). Using these diffusion velocities, we update the abundance of each species by solving Equations (5) and (9) together. We repeat this procedure through the mass accretion histories of galaxy clusters.

[4] Note that the Equation (16) provides a reasonable description of the MAHs of simulated galactic-size halos (Wechsler et al. 2002) by tuning a free parameter f to 0.254 (see Appendix A in van den Bosch 2002). For the cluster-size halos, we find that $f = 0.656$ provides a reasonable description of their MAHs and the average formation time of a large statistical samples of clusters-size halos extracted from N-body simulations (Cohn & White 2005, see also Berrier et al. 2008).

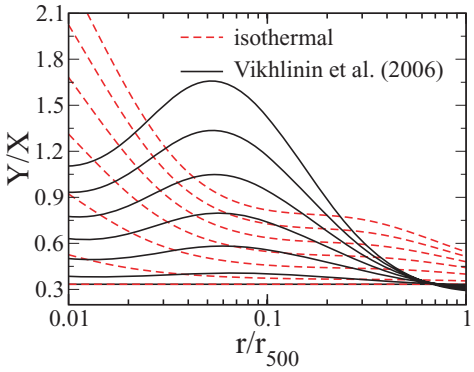

Figure 2. Spatial distribution of He-to-H mass fraction (Y/X) in a $T_X = 10$ keV static cluster with $f_B = 1$. Lines indicate two types of ICM temperature profiles shown in Figure 1. From the bottom to the top, the set of curves shown are for cluster ages of 0, 1, 3, 5, 7, 9, and 11 Gyr, respectively.

(A color version of this figure is available in the online journal.)

We use 600 spatial grids logarithmically spaced in a computational domain of $10^{-3} \leqslant r/r_{500} \leqslant 10$ and set the diffusion velocities to zero at both the inner and outer boundaries. These choices ensure that results are robust in regions of our interest ($0.01 < r/r_{500} \leqslant 1$).

Figure 2 shows the evolution of a spatial distribution of the He-to-H mass fraction (Y/X) of a $T_X = 10$ keV cluster with $f_B = 1$. Here we compare results of the isothermal model and those of the V06 model. This comparison shows that the observed temperature drop in the outer regions significantly suppresses the process of He sedimentation in the outskirts ($r/r_{500} > 0.3$) of clusters. The efficiency of He sedimentation, however, is enhanced in the inner regions near the peak of the observed temperature profile, and it is suppressed again in the innermost regions ($r/r_{500} < 0.02$) due to the observed temperature drop at these radii. At $r = r_{500}$, the He abundance in the V06 model is very close to the primordial value ($Y/X = 0.333$). The effect of He sedimentation is negligible at this radius, and these results are fairly independent of cluster age and the value of f_B. These conclusions are in stark contrast with the result of the isothermal model which gives considerably larger He abundance of $Y/X = 0.479$. In the V06 model, the value of Y/X increases rapidly toward inner regions and peaks at $r = 0.06\ r_{500}$. The mass fraction ratio increases to $Y/X = 0.405$ at $r = r_{2500}$ and 1.0 at $r = 0.1\ r_{500}$ for the cluster age of 7 Gyr.

4.2. Effect on Gas Mass, Total Mass, and Gas Mass Fraction

As we discussed in Section 2, the spatial variation in the He abundance caused by the mass segregation could introduce observational biases in X-ray measurements of galaxy clusters. Figure 3 shows biases in X-ray measurements of gas mass, total mass, and gas mass fraction at r_{2500} for three sedimentation models: the isothermal model with $f_B = 1$ (dashed line), the V06 model with $f_B = 1$ (thick-solid line) and $f_B = 5$ (thin-solid line). Results are shown for a typical cluster age of 7 Gyr and for a range of average cluster temperatures ($T_X = 1-10$ keV). Here we define these biases to be ratios between the quantities derived by assuming the primordial abundance and their true values in our cluster models, which correspond to the values that would have been obtained if the sedimentation effect was taken into account in X-ray data analyses.

Comparing results of two different models, we find that biases in X-ray measurements of total cluster mass at r_{2500} are

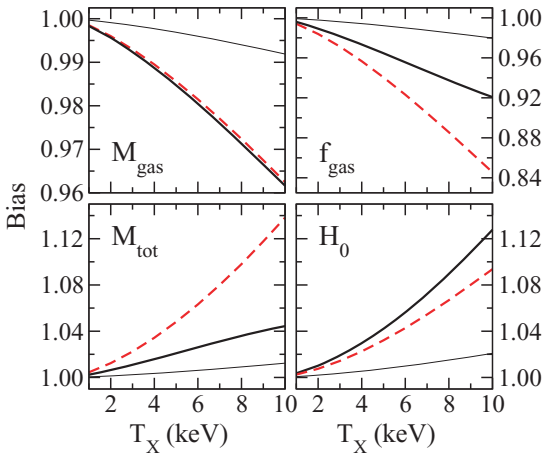

Figure 3. Biases in X-ray measurements of galaxy clusters at r_{2500} as a function of T_X for a static cluster age of 7 Gyr. Lines indicate the isothermal model (dashed line) and the V06 model with $f_B = 1$ (thick solid line) and $f_B = 0.2$ (thin solid line).

(A color version of this figure is available in the online journal.)

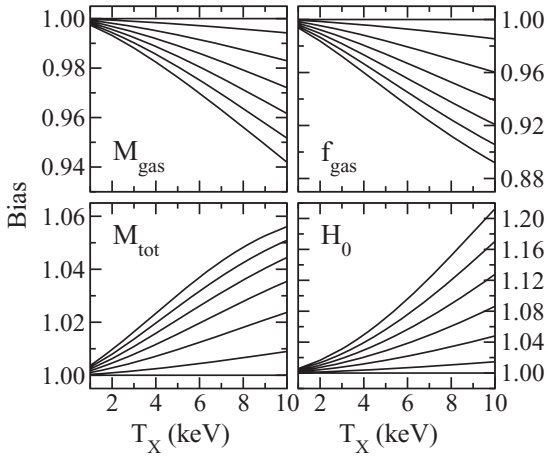

Figure 4. Biases in X-ray measurements of galaxy clusters r_{2500} as a function of cluster age. The curves starting from the flat line corresponds to cluster ages of 0, 1, 3, 5, 7, 9, and 11 Gyr. Results are shown for static clusters of the V06 model with $f_B = 1$.

considerably smaller in the V06 model. In the case of a hot ($T_X = 10$ keV), unmagnetized ($f_B = 1$) cluster, for example, the total mass is overestimated by 4% and 14% for the V06 model and isothermal model, respectively. The biases in $M_{\rm gas}$, on the other hand, are underestimated by 4% for both models. Note that these values are similar for two different temperature models. This is because $M_{\rm gas}$ measurements, obtained by integrating the gas density over the cluster volume, depend primarily on the average ICM temperature (T_X), and are relatively insensitive to the details of ICM temperature profiles. $f_{\rm gas}$ is then biased low by 8% and 16% for the V06 model and the isothermal model, respectively. Note that the bias in $f_{\rm gas}$ above is obtained by integrating from the cluster center to the radius r. This yields a large bias than that evaluated by using the local He abundance at r (Markevitch 2007).

The biases in X-ray measurements are very sensitive to the average ICM temperature (T_X) as well as the magnetic suppression factor (f_B). The biases are considerably smaller in cluster with smaller values of T_X or f_B, because the sedimentation process is slow in these clusters with larger resistance coefficients. We find that the biases at r_{2500} become negligible ($\lesssim 2\%$) for $T_X \lesssim 3$ keV or $f_B \lesssim 0.2$. These biases also depend sensitively on the age of clusters. Figure 4 illustrates that these biases increase rapidly with the cluster age and cause the apparent evolution of X-ray measurements of hot, dynamically relaxed clusters. Our sedimentation model based on the observed V06 temperature profile predicts that the biases in $f_{\rm gas}$ are likely less than 10% for a realistic range of cluster parameters (including the cluster age, T_X, and f_B). Note also that the biases become negligible in cluster outskirts ($r \sim r_{500}$) for all systems.

4.3. X-Ray and SZE-Derived Hubble Constant

Measurements of angular diameter distance derived from the combination of X-ray and SZE observations also depend on the assumed He abundance, x, as

$$d_{\rm A} \propto \frac{y^2}{S_X T_e^2} \frac{1+4x}{1+2x}, \qquad (17)$$

where the expression was obtained by canceling electron densities in both the X-ray surface brightness $S_X \propto n_e^2 d_A (1+4x)/(1+2x)$ (see Equation (2)) and the SZE Comptonization parameter $y \propto n_e T_e d_A$. Since $H_0 \propto d_A^{-1}$, the X-ray+SZE derived H_0 measurements could be affected by the He sedimentation process. As shown in the bottom right panels of Figures 3 and 4, our model suggests that the sedimentation could introduce biases in the X-ray+SZE derived H_0 measurements high by about $\lesssim 15\%$, with the exact value depending on the cluster age, temperature, as well as the magnetic suppression factor. This effect is of the same sign and order as the 6% offset seen between the X-ray and SZE-derived Hubble constant ($H_0 = 77.6^{+4.8}_{-4.3}$ km s^{-1} Mpc^{-1}) (Bonamente et al. 2006) and result of the Hubble Key Project ($H_0 = 73$ km s^{-1} Mpc^{-1}) (Freedman et al. 2001). Given the errors in the current X-ray+SZE H_0 measurements, our models with $f_B = 1$ and 0.2 are both consistent with the observed offset. As proposed by Markevitch (2007), the comparison of the X-ray+SZE derived H_0 and independent H_0 measurements could be used to constrain the He abundance in clusters.

4.4. Evolution of Cluster Gas Mass Fraction

The evolution of cluster gas mass fraction of X-ray luminous, dynamically, relaxed clusters can provide powerful observational constraints on the equation of state of dark energy w (Sasaki 1996; Pen 1997; Ettori et al. 2003; Allen et al. 2004; LaRoque et al. 2006, 2008). The sensitivity to w lies in the dependence of the observed $f_{\rm gas}$ to the angular diameter distance, $d_{\rm A}(w, z)$,

$$f_{\rm gas}(w, z) = 0.113 \left[\frac{d_{\rm A}(w, z)}{d_{\rm A}(w = -1.0, z)} \right]^{1.5}, \qquad (18)$$

where the observed $f_{\rm gas}$ is 0.113 at $z = 0$. Recent measurements of the $f_{\rm gas}$ evolution based on *Chandra* X-ray observations of 42 bright, dynamically relaxed galaxy clusters yielded $w = -1.14 \pm 0.31$, by assuming a flat geometry and standard priors on $\Omega_b h^2$ and h. The combined analysis of $f_{\rm gas}$ plus CMB and SNIa measurements constrains w to better than 10%, $w = -0.98 \pm 0.07$ (Allen et al. 2008).

Here we point out that the effect of He sedimentation can introduce an apparent evolution in X-ray measurements of cluster gas mass fractions, which could lead to systematic biases in observational constraints on the dark energy equation of state, w. This is illustrated in Figure 5, where we show evolution of the

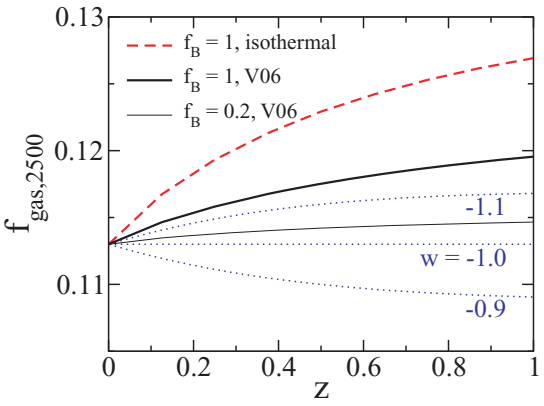

Figure 5. Evolution of cluster gas mass fraction enclosed within r_{2500} as a function of redshift. Results are for a 10 keV cluster with realistic MAHs given by Equation (16). Lines indicate the isothermal model with $f_B = 1$ (dashed line), V06 model with $f_B = 1$ (thick solid line) and $f_B = 0.2$ (thin solid line). Dotted lines indicate the evolution in f_{gas} caused by changes in the dark energy equation of state w by 10% relative to the fiducial ΛCDM cosmological model with no sedimentation (indicated with a straight dotted line).

(A color version of this figure is available in the online journal.)

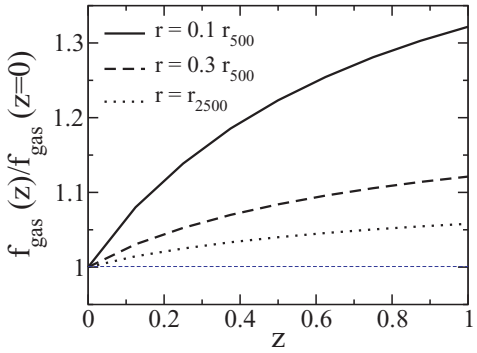

Figure 6. Evolution of cluster gas mass fraction enclosed within three cluster-centric radii, $r = 0.1\ r_{500}$ (solid lines), $r = 0.3\ r_{500}$ (dashed lines), and $r = r_{2500}$ (dotted lines). Results are for a 10 keV cluster with realistic MAHs given by Equation (16), for the V06 model and $f_B = 1$.

observed gas mass fraction at r_{2500} by using the realistic, time-dependent MAHs given by Equation (16) in order to follow the He sedimentation process in a growing cluster-size halo, starting from a protocluster at $z = 5$. Our sedimentation models show that the observed gas mass fraction is overestimated by 12%, 6%, and 2% at $z = 1$, for the isothermal model with $f_B = 1$, V06 model with $f_B = 1$ and $f_B = 0.2$, respectively. The apparent evolution in f_{gas} arises because clusters at lower redshifts have had more time to experience the sedimentation on average.

As shown in Figure 5, the effect of He sedimentation is degenerate with changes in the dark energy equation of state, w. Note that the changes in w by -10% (relative to the fiducial ΛCDM cosmology with $w = -1$) correspond to the changes in f_{gas} by about 3% between $z = 0$ and 1. The effect of He sedimentation is to make the best fit w more negative, i.e., $w < -1$. For example, results of the V06 model with $f_B = 1$ (0.2) are degenerate with the cosmological models with $w = -1.18$ (-1.04) without sedimentation. The isothermal model with $f_B = 1$, which should be taken as an extreme case, requires $w = -1.38$. Given the measurement uncertainties ($\approx 30\%$ in w), current constraints on w should not be affected significantly by the effect of He sedimentation. However, future X-ray measurements aiming to constraint w to better than 10% will need to take this effect into account. Note that the effect would be larger for a population of dynamically relaxed clusters than the average population considered here.

Given that the variation in the He abundance in clusters are unknown at present, it would be interesting to ask whether the current X-ray data could be used to constrain the abundance distribution. Here we propose that the f_{gas} evolution in the inner cluster regions, where the effect of sedimentation is expected to be larger, can be used as sensitive probes of the He sedimentation process. In Figure 6, we illustrate evolution of f_{gas} (V06 model with $f_B = 1$) at three different radii, including $r = 0.1\,r_{500}$, $0.3\,r_{500}$, and r_{2500}. This figure shows that changes in f_{gas} between $z = 0$ and 1 are amplified significantly in the inner regions of clusters. At $r = 0.1\,r_{500}$, f_{gas} evolves by $\sim 30\%$ from $z = 0$ to 1, which could be detected with current data. If the gas mass fraction evolution is detected, it can provide unique constraints on the efficiency of He sedimentation, which in turn provides constraints on the magnetic and turbulent suppression of particle diffusion in the weakly magnetized ICM. Nondetection is also interesting, as it will provide an upper limit on the efficiency of particle diffusion in the ICM.

5. DISCUSSIONS

Here we comment on additional effects that may affect our sedimentation calculations. First, turbulent mixing will likely play an important role in determining the efficiency of sedimentation. Turbulence, on the one hand, will tend to mix fluid elements from different parts of the cluster and to counteract the effect of sedimentation, but it may also enhance the rate of sedimentation by increasing the mobility of the ions. Detailed investigation of the effect of turbulence on the sedimentation process is beyond the scope of the present work. But, we point out that recent hydrodynamical simulations of galaxy cluster formation uniformly indicate the presence of ubiquitous subsonic turbulent flow in clusters (Norman & Bryan 1999; Nagai et al. 2003, 2007; Rasia et al. 2004, 2006; Kay et al. 2004; Faltenbacher et al. 2005; Dolag et al. 2005). These simulations indicate that the turbulence can provide about 5–10% of the total pressure support at $r = r_{500}$ even in relaxed systems, and its relative importance increases in cluster outskirts as well as unrelaxed clusters with recent major mergers (Lau, A. V. Kravtsov, D. Nagai, in preparation). It is therefore possible that turbulent mixing caused by gas accretion in cluster outskirts and/or major mergers may significantly modify the efficiency of the sedimentation. Hydrodynamical cluster simulations that also include the sedimentation physics will likely provide realistic assessment of this effect.

We also point out that the standard diffusion equations are valid only if the mean free path of the ions is small compared to the size of the computational zone used to solve these equations. The proton mean free path, however, could become a sizable fraction of the cluster size in cluster outskirts in some of our models (e.g., the unmagnetized case), which makes the fluid approximation invalid. We therefore carried out resolution studies and showed that our main results are not significantly affected by this problem.

In this work, we also neglected the effect of thermal diffusion, which can cause a change in the diffusion speed. To assess the effect of thermal diffusion, we follow the formalisms presented in Burgers (1969) which take into account the heat flow interferences, and apply it to the H–He plasma in the ICM. For the isothermal case, the diffusion velocity is enhanced by $\sim 23\%$, which agrees with the value reported by Chuzhoy

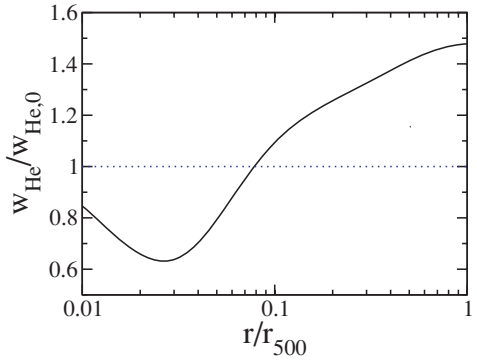

Figure 7. Ratio of two He sedimentation velocities derived with (w_{He}) and without ($w_{He,0}$) the effect of thermal diffusion, plotted as a function of the cluster-centric radius.

(A color version of this figure is available in the online journal.)

& Loeb (2004). For the nonisothermal case, we find that the thermal diffusion enhances the He sedimentation in the outskirts where the temperature gradient is negative, but suppresses the He sedimentation in the inner region ($r/r_{500} < 0.1$) with a positive temperature gradient. Our analysis indicates that the contribution of thermal diffusion to the diffusion velocity by about less than 50% throughout clusters. Figure 7 shows the change in the He sedimentation speed caused by the effect of thermal diffusion as a function of r/r_{500}. Note that the thermal diffusion causes a relatively small change in the Y/X at cluster outskirts (e.g., $r \sim r_{500}$), despite its large fractional change in diffusion velocity. It is because the diffusion speed was very small there to start with. Using the scaling of Y/X with time given by Chuzhoy & Loeb (2004), we find that the effect of thermal diffusion on Y/X is less than 20%.

It has been suggested that the enhancement of He abundance in the central regions might cause the decline of the observed Fe abundance (Ettori & Fabian 2006). To assess this effect, we repeat the He sedimentation calculations for the three cool-core clusters (including Centaurus, A2199, A1795) presented in Ettori & Fabian (2006), using their observed gas density and temperature profiles. Our calculations indicate that the enhancement of He in the core of the Centaurus cluster is less than 20% from the primordial He abundance, even in the extreme case of an unmagnetized cluster with a cluster age of 11 Gyr. This corresponds to a decline of the observed Fe abundance by only 7% (see Figure 4 of Ettori & Fabian 2006). Similar results are found for A2199 and A1795. Note that the He sedimentation is significantly suppressed in the cool-core regions. We thus conclude that the observed 20–50% reduction in the iron abundance in some of the cool-core clusters cannot be explained by the He sedimentation alone.

6. CONCLUSIONS

In this work, we investigate effects of He sedimentation on X-ray measurements of galaxy clusters and their implication for cosmological constraints derived from these observations. By solving a set of flow equations for a H–He plasma and using observationally motivated cluster models, we show that the efficiency of He sedimentation is significantly suppressed in the cluster outskirts due to the observed temperature drop, while it is dramatically enhanced in the cluster-core regions. Our sedimentation model based on the observed temperature profile suggests that the effect of helium sedimentation is negligible at r_{500}, and it does not affect cluster mass measurements obtained at a sufficiently large cluster radius. However, the effect of sedimentation increases toward the inner regions of clusters and introduces biases in X-ray measurements of galaxy clusters. For example, at r_{2500}, biases in X-ray measurements of gas mass, total mass, and gas mass fractions, are at the level of 5–10%. The effect of He sedimentation could also introduce biases in the estimate of the Hubble parameter derived from the combination of X-ray and SZE measurements, which could explain the observed offset in the X-ray+SZE derived H_0 and independent measurement from the Hubble Key project. We emphasize, however, that the magnitude of these biases depends sensitively on the cluster age, temperature, and magnetic and/or turbulent suppression in the ICM.

We show that the process of He sedimentation introduces apparent evolution in the observed gas mass fractions of X-ray luminous, dynamically relaxed clusters. The effect of He sedimentation could lead to biases in observational constraints of the dark energy equation of state w at a level of $\lesssim$10%. These biases tend to make the value of w more negative. Current measurements based on f_{gas} evolution (Allen et al. 2004, 2008) should not be significantly affected by these biases. However, future measurements aiming to constrain w to better than 10% may need to take into account the effect of He sedimentation. For cosmological measurements, one way to minimize these biases is to extend the X-ray measurements to a radius well beyond r_{2500}. At the same time, the evolution of cluster gas mass fraction in the inner regions of clusters should provide unique observational diagnostics of the He sedimentation process in clusters.

We thank Marc Kamionkowski, Andrey Kravtsov, Avi Loeb, Maxim Markevitch, and Sterl Phinney for useful comments on this work. We also acknowledge Avi Loeb for suggesting to consider the effect of turbulent mixing and the mobility of ions in the ICM. We thank the anonymous referee for helpful comments that greatly improved this work. This work is supported by Sherman Fairchild Foundation.

REFERENCES

Abramopoulos, F., Chanan, G. A., & Ku, W. H.-M. 1981, ApJ, 248, 429
Allen, S. W., Rapetti, D. A., Schmidt, R. W., Ebeling, H., Morris, R. G., & Fabian, A. C. 2008, MNRAS, 383, 879
Allen, S. W., Schmidt, R. W., Ebeling, H., Fabian, A. C., & van Speybroeck, L. 2004, MNRAS, 353, 457
Berrier, J. C., et al. 2009, ApJ, 690, 1292
Bonamente, M., Joy, M. K., LaRoque, S. J., Carlstrom, J. E., Reese, E. D., & Dawson, K. S. 2006, ApJ, 647, 25
Burgers, J. M. 1969, Flow Equations for Composite Gases (New York: Academic)
Chandran, B. D. G., & Maron, J. L. 2004, ApJ, 602, 170
Chapman, S., & Cowling, T. G. 1952, The Mathematical Theory of Non-Uniform Gases (Cambridge: Cambridge Univ. Press)
Cho, J., & Lazarian, A. 2004, J. Korean Astron. Soc., 37, 557
Chuzhoy, L., & Loeb, A. 2004, MNRAS, 349, L13
Chuzhoy, L., & Nusser, A. 2003, MNRAS, 342, L5
Cohn, J. D., & White, M. 2005, Astropart. Phys., 24, 316
Dolag, K., Vazza, F., Brunnetti, G., & Tormen, G. 2005, MNRAS, 364, 753
Ettori, S., & Fabian, A. C. 2006, MNRAS, 369, L42
Ettori, S., Tozzi, P., & Rosati, P. 2003, A&A, 398, 879
Faltenbacher, A., Kravtsov, A. V., Nagai, D., & Gottlöber, S. 2005, MNRAS, 358, 139
Freedman, W. L., et al. 2001, ApJ, 553, 47
George, M. R., Fabian, A. C., Sanders, J. S., Young, A. J., & Russell, H. R. 2009, MNRAS, in press (arXiv:0807.1130)
Gilfanov, M. R., & Syunyaev, R. A. 1984, Sov. Astron. Lett., 10, 137
Kay, S. T., Thomas, P. A., Jenkins, A., & Pearce, F. R. 2004, MNRAS, 355, 1091

Komatsu, E., et al. 2009, ApJS, 180, 330
LaRoque, S. J., Bonamente, M., Carlstrom, J. E., Joy, M. K., Nagai, D., Reese, E. D., & Dawson, K. S. 2006, ApJ, 652, 917
Lazarian, A. 2007, AIP Conf. Ser., 932, 58
Leccardi, A., & Molendi, S. 2008, A&A, 486, 359
Loeb, A. 2002, New Astron., 7, 279
Makino, N., Sasaki, S., & Suto, Y. 1998, ApJ, 497, 555
Mantz, A., Allen, S. W., Ebeling, H., & Rapetti, D. 2008, MNRAS, 387, 1179
Markevitch, M. 2007, ApJL, submitted (arXiv:0705.3289)
Markevitch, M., & Vikhlinin, A. 2007, Phys. Rep., 443, 1
Markevitch, M., et al. 2003, ApJ, 586, L19
Nagai, D., Kravtsov, A. V., & Kosowsky, A. 2003, ApJ, 587, 524
Nagai, D., Vikhlinin, A., & Kravtsov, A. V. 2007, ApJ, 655, 98
Narayan, R., & Medvedev, M. V. 2001, ApJ, 562, L129
Navarro, J. F., Frenk, C. S., & White, S. D. M. 1997, ApJ, 490, 493
Norman, M. L., & Bryan, G. L. 1999, in The Radio Galaxy Messier 87, ed. H.-J. Röser & K. Meisenheimer (Berlin: Springer), 530, 106
Parrish, I. J., Stone, J. M., & Lemaster, M. N. 2008, ApJ, 688, 905
Pen, U.-L. 1997, New Astron., 2, 309
Pratt, G. W., Böhringer, H., Croston, J. H., Arnaud, M., Borgani, S., Finoguenov, A., & Temple, R. F. 2007, A&A, 461, 71
Qin, B., & Wu, X. 2000, ApJ, 529, L1
Rasia, E., et al. 2006, MNRAS, 369, 2013
Rasia, E., Tormen, G., & Moscardini, L. 2004, MNRAS, 351, 237
Sasaki, S. 1996, PASJ, 48, L119
Spitzer, L. 1962, in Physics of Fully Ionized Gases, Physics of Fully Ionized Gases, (2nd ed.; New York: Interscience)
Tasitsiomi, A., Kravtsov, A. V., Gottlöber, S., & Klypin, A. A. 2004, ApJ, 607, 125
van den Bosch, F. C. 2002, MNRAS, 331, 98
Vikhlinin, A., Kravtsov, A., Forman, W., Jones, C., Markevitch, M., Murray, S. S., & Van Speybroeck, L. 2006, ApJ, 640, 691
Vikhlinin, A., et al. 2009, ApJ, in press (arXiv:0805.2206)
Wechsler, R. H., Bullock, J. S., Primack, J. R., Kravtsov, A. V., & Dekel, A. 2002, ApJ, 568, 52